

Rapid, high-resolution ^{14}C chronology of ooids

Steven R. Beaupré^{a,b*}, Mark L. Roberts^a, Joshua R. Burton^a, Roger E. Summons^c

- a. Dept. of Geology & Geophysics, Woods Hole Oceanographic Institution, Woods Hole, MA 02543, USA.
- b. School of Marine and Atmospheric Sciences, Stony Brook University, Stony Brook, NY 11794-5000, USA.
- c. Dept. of Earth, Atmospheric and Planetary Sciences, Massachusetts Institute of Technology, Cambridge, MA 02139, USA.

* Correspondence to
Steven R. Beaupré
email: steven.beaupre@stonybrook.edu
office: 631-632-3748

Abstract

Ooids are small, spherical to ellipsoidal grains composed of concentric layers of CaCO_3 that could potentially serve as biogeochemical records of the environments in which they grew. Such records, however, must be placed in the proper temporal context. Therefore, we developed a novel acidification system and employed an accelerator mass spectrometer (AMS) with a gas accepting ion source to obtain radiocarbon (^{14}C) chronologies extending radially through ooids within one 8-hour workday. The method was applied to ooids from Highborne Cay, Bahamas and Shark Bay, Australia, yielding reproducible ^{14}C chronologies, as well as constraints on the rates and durations of ooid growth and independent estimates of local ^{14}C reservoir ages.

1. Introduction

Ooids are small (< *ca.* 2 mm diameter), spherical to ellipsoidal grains of concentric layers of calcium carbonate (CaCO_3) that encase a nucleating fragment (Simone, 1980). Ooid laminations can also contain organic matter, and thus might conserve biogeochemical records of both the waters in which they grew and the microbial communities that colonize them during their formation (Edgcomb et al., 2013; Summons et al., 2013). However, in order to place their records in the proper temporal and biogeochemical contexts, the layers must be dated.

Radiocarbon (^{14}C ; half-life = 5730 ± 40 yr) is a powerful tracer of time that may be used to constrain the history of oolitic CaCO_3 assimilation. Previous measurements have demonstrated that ^{14}C ages of ooids decrease radially from their nuclei toward their outer surfaces. However, those pioneering studies were performed prior to the onset of modern radiocarbon dating conventions (Martin and Ginsburg, 1965), did not present sufficient methodological detail for replication (James et al., 2004), or were based on coarse radial resolution (Duguid et al., 2010; Hearty et al., 2010; James et al., 2004; Yokoyama et al., 2006). Therefore, we developed a new acidification method for measuring high-resolution radial ^{14}C chronologies of ooids. The method employed a unique accelerator mass spectrometry (AMS) system with a gas accepting ion source that reduced both the cost per ^{14}C measurement (by $\sim 1/3$; NOSAMS, 2013) and the total time for acidification and ^{14}C measurements (to ~ 8 hours). The method was applied to samples from two sites where ooids are presently forming: Carbla Beach, Australia and Highborne Cay, Bahamas. The resulting chronologies can be used to constrain the rates and durations of ooid growth, as well as the local ^{14}C reservoir ages of the seas in which they grew.

2. Methods

2.1. Samples

Two samples of ooids were collected by hand from surf zones (~ 1 m deep) of the windward side of Highborne Cay, Bahamas (24° 43' N, 76° 49' W) in March, 2010, and from Carbla Beach in Shark Bay, Australia (26° 9'40" S, 114°12'42" W) in June 2011. The samples were rinsed with deionized water, freeze dried, then doubly sieved to remove skeletal detritus and to partition the ooids into discrete particle size bins of 0.105 to 0.177 mm and 0.177 to 0.250 mm for Highborne Cay ooids, and 0.177 to 0.250 mm and 0.250 to 0.590 mm for Carbla Beach ooids. An additional size fraction (singly sieved, ≤ 0.250 mm) from Highborne Cay was used for preliminary tests of our methods. The samples were stored in pre-baked glass vials until analysis. Aliquots of ooids from each size class were then surveyed for variations in geometries and fractures with a table top electron microscope (TM3000, Hitachi).

2.2. Sample acidification and isotopic analysis

The average mass of carbonate-carbon in an individual ooid (~2 $\mu\text{g C-CaCO}_3$) approaches the theoretical detection limit for natural abundance ^{14}C measurements (~1 $\mu\text{g C}$) (Currie et al., 2000). Therefore, radial chronologies could not be constructed by directly measuring the ^{14}C ages of individual laminations within a single ooid. Alternatively, we measured the ^{14}C ages of large fractions of CO_2 (~324 $\mu\text{g C}$) collected successively during the continuous acidification of multiple ooids in a novel bubble column reactor system (Figure 1A).

Ooids (~35 mg C) were placed in the reactor (Figure 1B) and the system purged of residual CO_2 with 35 ml/min of ultra-high purity (UHP) helium that was continuously scrubbed with Ascarite-II (Thompson Scientific). The reaction was then initiated by injecting 5 ml of

dilute aqueous phosphoric acid [1 ml 85 % H_3PO_4 (Certified ACS grade, Fisher Scientific) in 99 ml Milli-Q water and exhaustively sparged with helium]. The resulting CO_2 was continuously sparged from the reactor by a stream of CO_2 -free UHP helium, and dried through a loop of ¼” OD stainless steel tubing (McMaster-Carr) immersed in a dry ice/isopropanol slush (-78°C). The concentration of CO_2 in the gas stream was monitored by a calibrated infrared CO_2 analyzer (Sable Systems CA-10A) and maintained between ~1000 and ~3000 ppm by drop-wise injections of 85 % H_3PO_4 . The CO_2 analyzer had been customized to reduce blanks and dead volumes by replacing the stock interior polymer tubing and aerosol filter with 1/8” OD copper tubing (McMaster-Carr) and a stainless steel fritted filter (Cat. No. ZBUFR2F, VICI Inc.). In addition, a custom LabVIEW (National Instruments Corp.) computer program continuously integrated the mass of carbon detected by the CO_2 analyzer and then directed the gas stream to one of three channels on the fraction collector.

Successive fractions of CO_2 (~324 $\mu\text{g C}$) were isolated inside novel, flow-through cryogenic traps (Figure 1C). The trap body consisted of a fire-polished borosilicate rod encased within a borosilicate tube (cut from Chemglass, CG-710-03L and CG-700-06L, respectively) that was capped at both ends by Shimadzu-style silicone plug septa (Restek, Cat#27171). The trap passed through a 7 mm diameter hole cored from the bottom of a Styrofoam drinking cup that held liquid nitrogen. The stream of helium and CO_2 emanating from the reactor was delivered to the bottom septum of each trap through flexible metal tubing (Cat No. 321-4-X-12, Swagelok) that terminated in 1” long 21-gauge deflected point needles (Cat No. 14-825-15T, Fisher Scientific) secured by Valco tube adapters (Cat No. ZTA41, VICI Inc.) and ¼” Ultra-Torr unions (Cat. No. SS-4-UT-6, Swagelok). A second needle connected the top septum of each trap to a glass manifold where residual helium was either i) vented to the atmosphere while trapping CO_2

or ii) removed from the trap by a turbo molecular pump (ATH 31, Alcatel). Successive fractions of CO₂ were thus isolated in the traps, pumped free of residual helium, removed from the manifold, and replaced with new traps by cycling the stream of helium and CO₂ through each of the three channels (Figure 1A).

The new trap was validated by measuring the transmittance of a gas standard (1000 ppm CO₂ in helium) flowing at 52 ml/min for 45 min (i.e., *ca.* 1200 µg C per test). Un-trapped CO₂ was quantified by two independent methods. First, a trap was vented to an open split monitored by a residual gas analyzer (RGA; Dycor LC Series, Ametek) and the entire system was purged overnight with CO₂-free helium to minimize the background. The trap was then chilled with liquid nitrogen and monitored while switching from a flow of CO₂-free helium to the gas standard. In the second approach, the gas standard was vented from the novel trap into a previously validated flow-through CO₂ trap (Rosenheim et al., 2008) instead of the RGA. The contents of the downstream trap were then isolated, pumped of non-condensable gases, cryogenically dried with a dry-ice/isopropanol slush, and quantified manometrically.

The ¹⁴C content of each fraction of CO₂ was quantified on the same day as the sample acidification via NOSAMS' gas ion source continuous flow accelerator mass spectrometry (GIS-CFAMS) system (Roberts et al., 2013b; Roberts et al., 2011), using a modified procedure to accommodate the new traps. Briefly, a syringe pump (NE-300, Syringepump.com) delivered 0.5 ml/min of CO₂-free, aqueous H₃PO₄ (pH ≤ 2) into the bottom of each cartridge via a 21-gauge deflected point needle. CO₂ was displaced from the top of each cartridge through the needle of a small open split and aspirated into the GIS-CFAMS through a fused silica capillary. The fractions of CO₂ were measured in random order to minimize potential bias from AMS normalization drifts. Each ~324 µg C fraction was counted for ~40 seconds with an associated

fraction modern (F_m) uncertainty of *ca.* < 0.02 (i.e., ± 1 standard deviation). All measurements were normalized and background corrected with modern and dead standard reference gases (Roberts et al., 2013a; Roberts et al., 2013b), and were reported (Table A.1) as both fraction modern and conventional radiocarbon ages based on the 5568 yr Libby half-life of ^{14}C (Stuiver and Polach, 1977).

Process blanks associated with ooid acidification were too small for direct ^{14}C measurement and therefore determined by standard additions. Briefly, separate traps were filled offline with modern and dead CO_2 standards during the acidification of each sample of ooids. The measured ^{14}C values of these standards were compared to those of the same modern and dead CO_2 standards prepared by the standard operating procedure for GIS-CFAMS analyses (Roberts et al., 2013a; Roberts et al., 2013b), with deviations attributed to a reproducible blank.

2.3. *Assembling ^{14}C chronologies*

The ^{14}C ages of individual CO_2 fractions collected during acidification were mapped to a sequence of concentric layers of carbonate within an individual, idealized ooid based on the following simplifying assumptions. First, all ooids were identical spheres of calcium carbonate cortices surrounding spherical non-carbonate nuclei. Second, identical layers of carbonate were simultaneously acidified from all ooids exclusively in sequence from the outermost- to the innermost layers. Third, the cortices were liberated quantitatively as CO_2 upon completion of the reaction. Therefore, the difference between the total mass of all ooids in a sample and the stoichiometrically equivalent mass of all CaCO_3 liberated as CO_2 by exhaustive acidification was attributed to the presence of stony nuclei and/or non-carbonate inclusions. Therefore, the residual mass represented an upper limit on the total mass of all non-carbonate nuclei in the sample and was expressed as a percentage (Table 1).

Accordingly, the average mass of carbonate-carbon (\overline{m}_i) in each spherical layer (i) was calculated from measurements of the mass of carbon collected in each fraction of CO₂ ($m_{f,i}$), the total mass of ooids in the sample (m_{sample}), their density prior to acidification (ρ_{ooid}), and the maximum ooid radius (R) as inferred from sieving (Eq. 1; see Appendix for derivations of equations).

$$\overline{m}_i = \rho_{ooid} \frac{m_{f,i}}{m_{sample}} \frac{4}{3} \pi R^3 \quad (1)$$

Since the conventional ¹⁴C age measurements (T_i) were, by definition, mass-weighted averages for all carbon atoms in each fraction, they were plotted against the median masses of each corresponding spherical layer of carbonate ($\overline{m}_{r,j}$).

$$\overline{m}_{r,j} = \frac{\overline{m}_j}{2} + \sum_{i=1}^j \overline{m}_{i-1} \quad (2)$$

In the absence of high-resolution particle size distributions, the radial chronologies were constrained by assuming two cases in which the initial ooid radii (R) were equal to either the larger or smaller sieve radius of each size bin.

Correlations between ¹⁴C ages and sample masses were determined by geometric mean least-squares linear regressions because both measurements possessed non-trivial uncertainties (Glover et al., 2011; Pataki et al., 2003). Geometric mean slopes were found by dividing the slopes of the conventional Model-I regressions (minimizing error in the dependent variable only) by their associated correlation coefficients (r). Geometric mean intercepts (b) were subsequently calculated from the linear equation $y = mx + b$ using geometric mean slopes (m) and average values of all respective x and y data.

3. Results and Discussion

3.1. System Performance

The acidification reactor (Figure 1) employed a bubble column to create a uniform suspension of ooids in acid. This approach minimized the risks of ooid fracturing and radiocarbon contamination anticipated for mechanical methods of stirring (e.g., magnetic spin bars). Two prototype reactors—based on traditional gas washing bottles—were visibly unable to loft most of the ooids and yielded noisy ^{14}C chronologies (not shown). These early results underscored the importance of uniform mixing in symmetric and synchronous digestion of all ooids in each sample. In the final version of the reactor (Figure 1), the tendency for ooids to settle was counteracted by the turbulent emanation of helium bubbles from all surfaces within a small fritted “basket” at the bottom of the reactor.

The second innovation that permitted rapid ^{14}C measurements by GIS-CFAMS was the flow-through trap (Figure 1C). The traps quantitatively isolated CO_2 from a helium stream based on the results of two different transmittance tests. First, an RGA did not detect CO_2 exiting the traps during 45 minutes of continuous trapping, even when the liquid nitrogen bath was allowed to fall to just ~2 mm depth. Second, a downstream trap collected only $2 \pm 1 \mu\text{g C}$ as CO_2 (manometrically quantified), representing $\leq 0.2\%$ of the total mass of carbon isolated during the tests. These high efficiencies were partly due to the presence of the inner glass rod, which maximized turbulence and contact with the cold outer glass walls of the trap (~0.5 mm wide annular space). They were also due to a stationary liquid nitrogen front where CO_2 entered the trap from below (Jordan, 1962). This design differs from traditional traps in which CO_2 enters from above and is alternately trapped and released as liquid nitrogen levels fluctuate through evaporation and refilling. Collectively, the gas flow rates, trapping durations, and masses of CO_2

isolated in these tests were more extreme than those employed during ooid acidification.

Therefore, the traps were deemed an effective means of collecting fractions of CO₂ released by the ooids.

The traps were less effective, however, at storing CO₂ for long periods of time. The pressure of CO₂ inside the traps steadily decreased following sample collection and thus reduced the effective storage time to 24 hours. The pressure drop was attributed to the diffusion of CO₂ into the silicone septa and could, in theory, be ameliorated with an alternative septum material. This limitation did not preclude our goal of measuring high-resolution ¹⁴C chronologies of ooids within one working day (≤ 8 hours), but the convenience of longer storage times warrants future modifications to the trap design. Alternatively, the CO₂ could be collected in a traditional cryogenic trap (e.g., Rosenheim et al., 2008), graphitized, and quantified by sputter ion source AMS for higher precision measurements (i.e., $\sigma_{Fm} \leq ca. \pm 0.005$ for pre-bomb samples).

Collectively, the ooid acidification system (Figure 1) did not produce detectable blanks ($< 0.2 \mu\text{g C}$, manometric) during the fraction collection process based on the mass of carbon that was collected when flowing CO₂-free helium through separate traps. Furthermore, student's t-tests demonstrated that the ¹⁴C values of modern and dead standards stored in the novel traps were indistinguishable from those prepared by the standard operating procedure for GIS-CFAMS. Thus, any additional errors due to extraneous carbon incorporated during sample collection or storage were assumed negligible for these analyses.

3.2. *Electron microscopy*

Electron microscope surveys (Figure 2) revealed that the samples were predominantly smooth ellipsoidal grains of roughly the same dimensions and therefore consistent, on average, with the idealized spherical ooid used to model their radial ¹⁴C chronologies. However, the

samples also contained a small proportion of ooids that were extensively fractured, bored, salt-encrusted, or cemented into larger aggregates. Some decidedly non-ellipsoidal grains and non-oolitic sediments were also observed. All of these particles deviated from the idealized ooid and introduced uncertainty into the presumed size distributions. For example, small ooids that were aggregated into larger particles or extensively encrusted with salt were not necessarily separated from the larger size class by sieving. Higher magnification of select ooids also revealed the formation of newer carbonates and the presence of microorganisms (e.g., diatoms) within surface fractures (Figure 3). In both cases, the heterogeneity in surface area, roughness, and carbon provenance throughout surface fractures were potential sources of additional uncertainty when constructing radial ^{14}C chronologies. Therefore, the measured fraction masses used in all calculations (Table A.1) were presumed to have an augmented relative uncertainty of $\pm 10\%$ to account for these variations. Nevertheless, more robust chronologies could be constructed by removing the rougher, highly eccentric, and non-oolitic particles prior to acidification, for example, by collecting only those grains which readily roll down a vibrating inclined plane (Martin and Ginsburg, 1965).

3.3. *Carbla Beach ooid chronology*

Conventional ^{14}C ages of CO_2 released during acidification increased steadily from “modern” to 1400 ± 280 yr in the smaller size class (0.177 to 0.250 mm diameter) and from 160 ± 140 yr to 1220 ± 160 yr in the larger size class (0.250 to 0.590 mm diameter) of Carbla Beach ooids (Table 1, Figure 4a). In both classes, ages of the outermost layers were significantly ($> 2\sigma$) younger than the nearest reported pre-bomb reservoir age (466 ± 31 yr, at 28.7°S , 113.8°E) from corals near the Western Australian coast (Squire et al., 2013). Unfortunately, there are no published reservoir ages within Shark Bay, making it difficult to apportion this ^{14}C enrichment

between bomb- ^{14}C and a naturally young pre-bomb reservoir age. Assuming a constant but unknown local reservoir age, the difference between initial and final fractions of CO_2 corresponded to the passing of approximately 1400 ± 280 conventional ^{14}C years since ooids in the smaller size class began to accrete carbonate. Likewise, the larger ooids accreted carbonate for approximately 1060 ± 210 conventional ^{14}C years.

The implications of these chronologies can be further explored by applying growth models for individual grains. The simplest models are empirical and assume constant net growth (i.e., carbonate assimilation – abrasion) with respect to either ooid mass or radius. However, selection of the most representative model was precluded by equally strong coefficients of determination for linear regressions of ^{14}C ages versus either mass or radius ($r^2 = 0.943$ and 0.944 , respectively, for the larger size class; $r^2 = 0.968$ and 0.968 , respectively, for the smaller size class) and measurement uncertainties. Therefore, the following analyses were based on the model of a constant net growth rate (k_m) with respect to mass of carbon because it provided a more meaningful intercept (^{14}C age limit) and relied on fewer assumptions, equations, and measurements (Eq. 3; Appendix A.2).

$$\overline{T}_j = T_{\max} - \frac{1}{k_m} \overline{m}_{r,j} \quad (3)$$

Although this simplified model does not explicitly contain geochemical or sedimentological factors that control ooid growth, it has high coefficients of determination, is appropriate given the GIS-CFAMS ^{14}C uncertainties ($\sim 2\%$ coefficient of variation), and provides additional insights into ooid growth rates, lifetimes, and the average ^{14}C reservoir ages of their local waters.

For example, the intercept (T_{\max}) of a linear regression between ^{14}C ages (\overline{T}_j) and masses of carbon ($\overline{m}_{r,j}$) suggested that, on average, idealized ooids in the larger size class had a

maximum age of 1240 ± 50 yr BP (± 1 standard error). Furthermore, the duration of their growth (“lifespan”) was calculated by subtracting the limiting ^{14}C age of the outermost, infinitesimally thin lamination (i.e., Eq. 3 at $\overline{m_{r,j}} = \sum \overline{m_i}$ for all $i = 1$ to N layers) from that of the innermost lamination (T_{max}) to be 1120 ± 210 yr. In comparison, linear regression of the smaller size class chronology ($r^2 = 0.943$) suggested a maximum age of 1310 ± 80 yr BP and a lifespan of 1470 ± 280 ^{14}C yr. These estimates represent the maximum range of ages between the infinitesimally thin inner and outer reaches of carbonate, rather than the attenuated ages of arbitrarily thick layers associated with the initial and final fractions of CO_2 . Furthermore, they were calculated independently of the presumed initial radius (R), ooid density (ρ_{ooid}), or the total mass of ooids in each sample (see Appendix A.3).

The lifespans calculated via Eq. 3 were also independent of the unknown reservoir age at Carbla Beach in Hamelin Pool. If the ooids were autochthonous and presently forming in waters with a constant reservoir age, then the maximum ^{14}C ages should have exceeded the lifespans by an amount equal to the reservoir age. Instead, they were within uncertainty of each other for each size class. This is possible if the local reservoir age was closer to 0 yr BP than the nearest reported reservoir age (466 ± 31 yr), which was measured outside of Shark Bay (Squire et al., 2013). Therefore, concordance between lifespans and maximum ^{14}C ages implies that the smaller ooids began assimilating carbonates approximately 1470 ± 280 yr BP, and the larger ooids began approximately 1120 ± 210 yr BP. Since these two estimates were not statistically different, we estimate that, on average, ooids in both size classes began growing at Carbla Beach approximately 1300 ± 200 yr BP.

If ooids collected from Carbla Beach were autochthonous, continuously created, and accumulating mass at a constant net rate, then we would have expected the smaller ooids to

possess similar net growth rates (i.e., slopes) but younger ^{14}C ages and shorter lifespans than the larger ooids (i.e., parallel linear ^{14}C chronologies). Instead, the smaller ooids appeared to have similar ages, longer lifespans, and net growth rates that were between 1.4 to 50 times slower than the larger ooids (Table 1). Explanations for this unanticipated result include, but are not limited to, actual size-dependent net growth rates (variations in the rates of assimilation and abrasion), contamination from fossil carbonate nuclei, or particle size distributions that peaked very near the diameter of the partitioning sieve (i.e., 0.250 mm). The latter two explanations relate to methodology and thus warrant further discussion.

First, the apparent longevity and slow net growth rates of smaller ooids may result from contamination by CO_2 released from fossil carbonate nuclei (e.g., ^{14}C -depleted forams or shell fragments). Such contamination would have to i) be a more pronounced characteristic of the smaller ooid size fraction, ii) possess a nearly constant ^{14}C age, and iii) comprise a nearly constant or \sim linearly increasing proportion of fossil C in each fraction of CO_2 in order to maintain the observed linearity in the ^{14}C chronologies. In addition, the combined proportion and ^{14}C age of fossil carbonate contamination in the smaller size class would have to yield similar ^{14}C ages of the innermost fractions of CO_2 in both size classes of ooids. While we cannot unambiguously rule out the influence of fossil carbonate nuclei, the combination of these constraints and the significant residual masses of non- CaCO_3 material [$\sim 40\%$ by weight (i.e., w/w), Table 1] suggests that the CO_2 was primarily derived from cortical carbonates.

Second, the apparent longevity and slower net growth rates of smaller ooids could have arisen from constraining their modeled radii with either the smaller or larger sieve diameters, rather than with high-resolution particle size distributions. For example, if the distribution of ooid radii peaked near the radius of the sieve that separated the two size classes (i.e., $2R = 0.250$

mm), then both size classes would have been dominated by similarly sized ooids, yielding nearly identical chronologies (not shown) and net growth rates (i.e., 1.0 ± 0.1 and 1.4 ± 0.1 ng C-CaCO₃ ooid⁻¹ yr⁻¹; Table 1). Such a distribution would also account for the nearly identical compositions of both size classes (Table 1) based on CO₂ yields (~7 % w/w), stoichiometrically equivalent proportions of CaCO₃ (~60 % w/w), and the proportions of residual non-carbonate material (~40 % w/w).

Alternatively, the seemingly faster net growth rate of the larger size class of ooids could be explained geochemically, rather than methodologically, by invoking size-dependent net growth rates. Regardless of the mechanism, this apparent acceleration should not have yielded the observed linear ¹⁴C chronologies unless i) the two size classes coincided with size-regimes that experienced different conditions, on average, during development but were collocated during sample collection, and/or ii) the combination of ¹⁴C uncertainty, net growth rates, and durations of growth precluded the detection of non-linearity. Indeed, the nearly identical proportion (40 % w/w) of non-carbonate material in both size classes implies that the larger ooids in this study grew from more massive nuclei and hence from potentially more massive nascent ooids than were found in the smaller size class. As such, the ooids in each size bin could have followed unique developmental trajectories. However, the methodological considerations noted above call for additional evidence before invoking the intriguing hypothesis of size-dependent net growth rates.

Ultimately, deviations from the underlying assumptions of ideal ooid geometry and composition could have yielded additional uncertainties in the measured ¹⁴C chronologies, limiting ages, and lifespans. For example, the diameters, compositions, and ages of ooid cortices and nuclei likely varied within each sample, and should have been associated with a spectrum of

radial chronologies and acidification kinetics curves. The ensuing time-dependent mixtures of CO₂ that evolved from the various carbonate laminations would thus have attenuated the range of observed ¹⁴C ages, implying artificially shorter average lifespans and faster apparent net growth rates. These sources of uncertainty are inherent to the simple model and preparation methods (e.g., sieving) employed here, are applicable to all samples in this study, and should be addressed in future studies before invoking geochemical explanations for unexpected observations. Much of this uncertainty could be reduced by measuring chronologies of ooids separated into higher resolution size bins, parameterizing their structural and compositional variations, and modeling the kinetics of their decomposition in acidic media.

3.4. *Highborne Cay ooid chronology*

Highborne Cay ¹⁴C chronologies were constructed under the same assumptions presented for Carbla Beach ooids (i.e., Eq. 1-3), but exhibited the following differences (Table 1, Figure 4b). First, the conventional ¹⁴C ages of CO₂ released from Highborne Cay ooids did not increase monotonically during acidification. Instead, there was an anomaly in which ¹⁴C ages became unexpectedly younger toward the interior of an idealized ooid. Second, the anomaly spanned nearly the same range of ¹⁴C ages in both size classes, suggesting that most of the ooids began growing, and continued to grow, in the same waters at the same time. Third, the chronology of the smaller size class did not continue toward modern values, but rather terminated abruptly following the ¹⁴C anomaly. Only one sample of the smaller size class exhibited near modern ages in the outermost layer (80 ± 120 yr), which then abruptly aged into the adjacent inner layer (480 ± 120 yr). These patterns could have emerged if the smaller ooids had stunted cortical growth after the anomaly, or if they were the remains of larger ooids whose outermost laminations have since abraded away.

The origin of the ^{14}C anomaly itself is uncertain. Severe weather has been observed to transport ooids onto beaches and into deeper waters (Major et al., 1996) where ooid growth is less likely to occur. However, such an occurrence would be expected to produce a step toward younger ages when ooids resumed growing, rather than the observed step toward older ages in the more distal laminations. Alternatively, the anomaly could have resulted from variations in the ^{14}C reservoir ages. Although this anomaly is not present on the Marine09 ^{14}C calibration curve, we cannot presently exclude the possibility of local changes in ^{14}C reservoir ages at Highborne Cay. The anomalously young interior ^{14}C ages could also have resulted from micritization by boring microorganisms and the subsequent incorporation of younger carbonates (Duguid et al., 2010; Edgcomb et al., 2013). Indeed, photomicrographs and fluorescently labeled core (FLEC) analyses have previously shown some Highborne Cay ooids to possess endolithic borings occupied by living microbes (Bernhard et al., 2003; Edgcomb et al., 2013). However, it is presently unclear why the ooids would produce an identical shift in ^{14}C ages that was more deeply embedded within the larger size fraction (Figure 4b). Finally, deviations from the idealized ooid geometry and composition could result in an anomaly. For example, a population of relict, thinly laminated ooids surrounding comparatively large nuclei could, in principle, have prematurely exhausted their supply of relatively old CO_2 during acidification and produced the step toward younger ages as the remaining younger ooids continued to decompose. Regardless of its origin, the anomaly was reproduced in both size classes, demonstrating fidelity in the ^{14}C record of these samples and precision in the acidification method.

These features preclude simple estimates of Highborne Cay ooid lifespans based on differences in ^{14}C ages of the innermost and outermost layers. Instead, only the outermost six fractions of the larger size class (0.177 to 0.250 mm) were subjected to a linear regression ($r^2 =$

0.926) because they aged monotonically. The intercept revealed a maximum age (T_{max}) of 1030 ± 80 years, which was corrected to 792 ± 80 yr BP assuming a local reservoir age of 238 ± 10 yr (Wagner et al., 2009) and thus concordant with the 800 ± 135 yr lifespan calculated via Eq. 3. Since both size classes i) possessed the same ^{14}C anomaly, ii) possessed the same ^{14}C ages (~ 965 yr BP, uncorrected) in their innermost fractions, and iii) the ^{14}C ages of their innermost fractions fell on the regression line (Fig 4), we conclude that ooids at this site began to accumulate carbonate, on average, at approximately the same time (~ 800 yr BP). Similar to Carbla Beach, it appears that ooids collected from Highborne Cay predominantly originated during a single event of some unknown duration.

Radiocarbon ages of the innermost ooid cortex layers have previously been observed to vary from 1023 to 2760 yr BP among multiple sites throughout the Bahamas (Duguid et al., 2010; Martin and Ginsburg, 1965). However, those pioneering results were based on different conventions and are not directly comparable with our results. For example, Martin and Ginsburg's (1965) chronology predated the ^{14}C reporting conventions of Stuiver and Polach (1977), was calculated via the 5730 yr "Cambridge" half-life (Godwin, 1962) rather than the 5568 yr "Libby" half-life, and reported relative to an internal standard. It is also unclear what, if any, reservoir age correction was applied. The beautiful suite of Bahamian chronologies reported by Duguid et al. (2010) were corrected with a local reservoir age anomaly ($\Delta R = 5$ yr, i.e., deviation from modeled global mean reservoir age) rather than the local reservoir age. In addition, their observed ranges of ^{14}C ages were likely accurate but attenuated by mass balance because each fraction comprised a larger percentage of the total mass of carbon per ooid. Nonetheless, the oldest ^{14}C age observed in the present chronology (970 ± 130 yr BP, without reservoir correction) was comparable to that reported by Duguid et al. (2010) from nearby

Ambergris Cay (1023 ± 36 yr BP). In addition, Duguid et al. (2010) reported an age of 413 ± 36 yr for the outermost 32 % of ooid mass, which is within uncertainty of the 390 ± 70 yr age calculated by mass balance for the outermost 34 % of our larger size class. Hence, in addition to the accurate and precise isotope ratios obtained for standards, reproducible and historically consistent ranges of ^{14}C ages within ooids of the Bahamian archipelago substantiate this method as a means to extract chronologies from ooids with isotopic fidelity.

4. Conclusions

The method employed here was capable of generating high-resolution, low cost, reproducible radial ^{14}C chronologies of ooids, each within an 8-hour workday. This approach exposed features, such as the ^{14}C anomaly at Highborne Cay and the possibility of size-dependent net growth rates at Carbla Beach, that suggest future lines of investigation into the details of ooid formation but which otherwise might have been obscured in lower resolution chronologies. Furthermore, the difference between maximum ages (T_{max}) and lifespans obtained from linear regressions provided an independent confirmation of the mean, local pre-bomb reservoir age at Highborne Cay and an estimation of the reservoir age at Shark Bay.

The ^{14}C chronologies obtained by this method, and thus our ability to interpret them, could be enhanced by sorting bulk ooid samples into higher resolution size bins, carefully selecting intact particles, parameterizing their structural and compositional variations, and modeling their decomposition in acidic media. The method could also be adapted for higher resolution chronologies, complementary chemical or isotopic analyses, and higher precision graphite sputter AMS ^{14}C measurements. Finally, the net growth rate model employed here was empirical and did not explicitly include factors that control the growth of individual grains. A

more realistic ooid growth model could be developed and tested by combining the above methodological improvements with chronologies from multiple sites, ultimately leading to better assessments of growth patterns, reservoir ages, and the geochemical records preserved within ooid cortices.

Acknowledgements

We thank Aimiee Gillespie for the ooid preparation, Malcolm Walter, Sabine Mehay, Pieter Visscher, Joan Bernhard and Ginny Edgcomb for logistical support of the sample collections, Horst Marschall for microscopy support, Bill Jenkins and the NOSAMS staff for technical support, and the reviewers and editors Mark Norman and Frank McDermott for their helpful comments. This work was financially supported by a National Science Foundation (NSF) grant to RES (OCE-0926372) and a NSF Cooperative Agreement with NOSAMS (OCE-2310753487). Work at MIT was also supported by an award (NNA13AA90A) from the NASA Astrobiology Institute.

References

- Bernhard, J.M., Visscher, P.T. and Bowser, S.S. (2003) Submillimeter life positions of bacteria, protists, and metazoans in laminated sediments of the Santa Barbara Basin. *Limnol. Oceanogr.* 48, 813-828.
- Brenninkmeijer, C.A.M. and Louwers, M.L. (1985) Vacuum-actuated high-vacuum glass valve. *Anal. Chem.* 57, 960-960.
- Currie, L.A., Kessler, J.D., Marolf, J.V., McNichol, A.P., Stuart, D.R., Donoghue, J.C., Donahue, D.J., Burr, G.S. and Biddulph, D. (2000) Low-level (submicromole) environmental ^{14}C metrology. *Nuclear Instruments & Methods in Physics Research, Section B - Beam Interactions With Materials and Atoms* 172, 440-448.
- Duguid, S.M.A., Kyser, K.T., James, N.P. and Rankey, E.C. (2010) Microbes and Ooids. *Journal of Sedimentary Research* 80, 236-251.
- Edgcomb, V.P., Bernhard, J.M., Beaudoin, D., Pruss, S., Welander, P.V., Schubotz, F., Mehay, S., Gillespie, A.L. and Summons, R.E. (2013) Molecular indicators of microbial diversity in oolitic sands of Highborne Cay, Bahamas. *Geobiology* 11, 234-251.
- Glover, D.M., Jenkins, W.J. and Doney, S.C. (2011) *Modelling Methods for Marine Science*, first ed. Cambridge University Press, Cambridge, UK.
- Godwin, H. (1962) Half-life of Radiocarbon. *Nature* 195, 984.
- Hearty, P.J., Webster, J.M., Clague, D.A., Kaufman, D.S., Bright, J., Southon, J. and Renema, W. (2010) A pulse of ooid formation in Maui Nui (Hawaiian Islands) during Termination I. *Marine Geology* 268, 152-162.
- James, N.P., Bone, Y., Kyser, K.T., Dix, G.R. and Collins, L.B. (2004) The importance of changing oceanography in controlling late quaternary carbonate sedimentation on a high-energy, tropical, oceanic ramp: north-western Australia. *Sedimentology* 51, 1179-1205.
- Jordan, A. (1962) An improved liquid nitrogen trap. *Journal of Scientific Instruments* 39, 447-448.
- Major, R.P., Bebout, D.G. and Harris, P.M. (1996) Recent evolution of a Bahamian ooid shoal: Effects of Hurricane Andrew. *GSA Bulletin* 108, 168-180.
- Martin, E.L. and Ginsburg, R.N. (1965) Radiocarbon ages of oolitic sands on Great Bahama Bank, *Proceedings of the Sixth International Conference on Radiocarbon and Tritium Dating*, Pullman, WA, pp. 7-11.
- NOSAMS, W.H.O.I. (2013) Fees for radiocarbon analyses, <http://www.whoi.edu/nosams/fees>, Woods Hole, MA.

- Pataki, D.E., Ehleringer, J.R., Flanagan, L.B., Yakir, D., Bowling, D.R., Still, C.J., Buchmann, N., Kaplan, J.O. and Berry, J.A. (2003) The application and interpretation of Keeling plots in terrestrial carbon cycle research. *Global Biogeochem. Cycles* 17, 1022, doi:10.1029/2001GB001850.
- Roberts, M.L., Beaupré, S.R. and Burton, J.R. (2013a) A high-throughput low-cost method for analysis of carbonate samples for ^{14}C . *Radiocarbon* 55, 585-592.
- Roberts, M.L., von Reden, K.F., Burton, J.R., McIntyre, C.P. and Beaupré, S.R. (2013b) A gas-accepting ion source for Accelerator Mass Spectrometry: Progress and applications. *Nuclear Instruments and Methods in Physics Research Section B: Beam Interactions with Materials and Atoms* 294, 296-299.
- Roberts, M.L., von Reden, K.F., McIntyre, C.P. and Burton, J.R. (2011) Progress with a gas-accepting ion source for Accelerator Mass Spectrometry. *Nuclear Instruments and Methods in Physics Research B* 269, 3192-3195.
- Rosenheim, B.E., Day, M.B., Domack, E., Schrum, H., Benthien, A. and Hayes, J.M. (2008) Antarctic sediment chronology by programmed-temperature pyrolysis: Methodology and data treatment. *Geochemistry Geophysics Geosystems* 9, 1-16.
- Simone, L. (1980) Ooids: a review. *Earth-Science Reviews* 16, 319-355.
- Squire, P., Joannes-Boyau, R., Scheffers, A.M., Nothdurft, L.D., Hua, Q., Collins, L.B., Scheffers, S.R. and Zhao, J.-x. (2013) A marine reservoir correction for the Houtman-Abrolhos Archipelago, East Indian Ocean, Western Australia. *Radiocarbon* 55, 103-114.
- Stuiver, M. and Polach, H.A. (1977) Discussion: Reporting of ^{14}C data. *Radiocarbon* 19, 355-363.
- Summons, R.E., Bird, L.R., Gillespie, A.L., Pruss, S.B., Roberts, M. and Sessions, A.L. (2013) Lipid biomarkers in ooids from different locations and ages: evidence for a common bacterial flora. *Geobiology* 11, 420-436.
- Wagner, A.J., Guilderson, T.P., Slowey, N.C. and Cole, J.E. (2009) Pre-bomb surface water radiocarbon of the Gulf of Mexico and Caribbean as recorded in hermatypic corals. *Radiocarbon* 51, 947-954.
- Yokoyama, Y., Purcell, A., Marshall, J.F. and Lambeck, K. (2006) Sea-level during the early deglaciation period in the Great Barrier Reef, Australia. *Global and Planetary Change* 53, 147-153.

Table 1: Ooid compositions, net growth rates, and lifespans ^a

	Highborne Cay, Bahamas		Carbla Beach, Australia	
	0.105 to 0.177	0.177 to 0.250	0.177 to 0.250	0.250 to 0.590
Size class (mm)				
% C (w/w)	8.1 ± 0.3	8.4 ± 0.3	7.1 ± 0.2	7.3 ± 0.3
% CaCO ₃ (w/w)	67 ± 2	70 ± 2	59 ± 2	61 ± 2
% non-CaCO ₃ matter (w/w)	33 ± 2	30 ± 2	41 ± 2	39 ± 2
Oldest measured fraction (¹⁴ C years)	960 ± 120	970 ± 130	1400 ± 280	1220 ± 160
Youngest measured fraction (¹⁴ C years)	80 ± 120	280 ± 130	Modern	160 ± 140
Observed age difference (¹⁴ C years)	N/A	690 ± 180	1400 ± 280	1060 ± 210
Bulk ¹⁴ C age ^b (¹⁴ C years)	580 ± 30 ^c	590 ± 45	570 ± 100	670 ± 60
Maximum age ^d of inner CO ₃ (¹⁴ C years)	N/A	1030 ± 80 ^e	1310 ± 80	1240 ± 50
Mean lifespan ^f (¹⁴ C years)	N/A	800 ± 135 ^e	1470 ± 280	1120 ± 210
Maximum net growth rate ^g (ng C-CaCO ₃ / ooid / yr)	N/A	2.2 ± 0.3	1.0 ± 0.1	18 ± 1
Minimum net growth rate ^h (ng C-CaCO ₃ / ooid / yr)	N/A	0.8 ± 0.1	0.36 ± 0.03	1.4 ± 0.1

^a All uncertainties reported as ± 1 standard deviation. ¹⁴C ages reported here were not corrected for local reservoir ages—see text for details and the appendix for original measurements (Table A1).

^b Calculated by mass balance from fraction modern values of all individual fractions.

^c Average for two trials with propagated uncertainties.

^d Intercept of the linear regression between ¹⁴C age and mass.

^e Based on linear regression through 6 outermost data points, only.

^f Based on the average mass per ooid and the slope of the linear regression between ¹⁴C and mass.

^g Based on the slope of the linear regression between ¹⁴C and mass, assuming initial ooid radius was equal to the larger sieve radius.

^h Based on the slope of the linear regression between ¹⁴C and mass, assuming initial ooid radius was equal to the smaller sieve radius.

Figure Captions

Figure 1: Ooid acidification system. (A) Schematic of the acidification reactor and trapping system. Arrows denote the direction of gas flow, and \otimes represent vacuum actuated glass valves (Part# 40.550.3, Louwers Glass and Ceramic Technologies; Brenninkmeijer and Louwers, 1985) that were controlled by the LabVIEW program. The reactor was plumbed to the helium source and trapping system with ¼” copper tubing via ¼” Ultra-Torr unions (#SS-4-UT-6, Swagelok; not shown). All injections were performed with 10 ml polypropylene luer-lock syringes and 21-gauge needles (Cat. No. 309604 and 305167, BD Co). (B) Reactor detail. The reactor was constructed from standard wall borosilicate tubing (Chemglass). A hollow medium-porosity fritted bubbler (gray) was triple sealed to the bottom and encased in a glass bulb, while a second glass bulb near the top of the reactor body prevented rising bubbles from exiting the reactor. The reactor was capped with a rubber septum (orange) taken from a Covidien Monoject 2 ml blood vial (Cat#: 22-029-319, Fisher Scientific). A solid glass strut (shown in black) was welded to the side arm for additional support. (C) Long-section of the cryogenic traps. The glass tube was capped at both ends by Shimadzu-style silicone plug septa (blue), and passed through a hole cored from the bottom of a Styrofoam drinking cup (black). A small bead of water (dark gray) placed around the hole quickly froze upon filling the cup with liquid nitrogen to form a leak-proof, but temporary, seal.

Figure 2: Electron microscope images of select particles that deviated from the form of an “ideal” ooid. (A) non-ellipsoidal particles, (B) boring, and (C) cratering in the sample of Highborne Cay ooids; (D) aggregates, (E) salt crusts, and (F) non-oolitic particles (i.e., foram) in the sample of Carbla Beach ooids.

Figure 3: Electron microscope images of two fractured Carbla Beach ooids with progressively magnified fields of view (A to C, and D to F), demonstrating surface damage, crystallization, and associated microorganisms (e.g., diatom in panel F).

Figure 4: Radial ^{14}C chronologies of ooids from (A) Carbla Beach, Australia and (B) Highborne Cay, Bahamas, as a function of the mass of carbonate-carbon extending radially from their interiors. Horizontal “error” bars span the mass of carbon per ooid collected from each layer, with conventional ^{14}C ages plotted at their midpoints. Vertical error bars represent ± 1 standard deviation in conventional ^{14}C ages. Ooids ranged in diameter from 0.105 to 0.177 mm (replicate analyses denoted by Δ and \circ), 0.177 to 0.250 mm (\bullet), ≤ 0.250 mm (\circ), and 0.250 to 0.590 mm (\blacksquare). Geometric mean linear regressions (black lines) in (A) were calculated from all ooids in each size class (\bullet , $r^2 = 0.943$, slope = $-995 \pm 90 \text{ yr } \mu\text{g-C}^{-1}$, intercept = $1314 \pm 103 \text{ yr}$), \circ ($r^2 = 0.968$, slope = $-56 \pm 4 \text{ yr } \mu\text{g-C}^{-1}$, intercept = $1238 \pm 46 \text{ yr}$), while those in (B) were calculated from only the 6 outermost layers of ooids with diameters between 0.177 and 0.250 mm (\bullet , $r^2 = 0.926$, slope = $-460 \pm 62 \text{ yr } \mu\text{g-C}^{-1}$, intercept = $1034 \pm 75 \text{ yr}$). Note that the scales on the radial mass axes differ between (A) and (B).

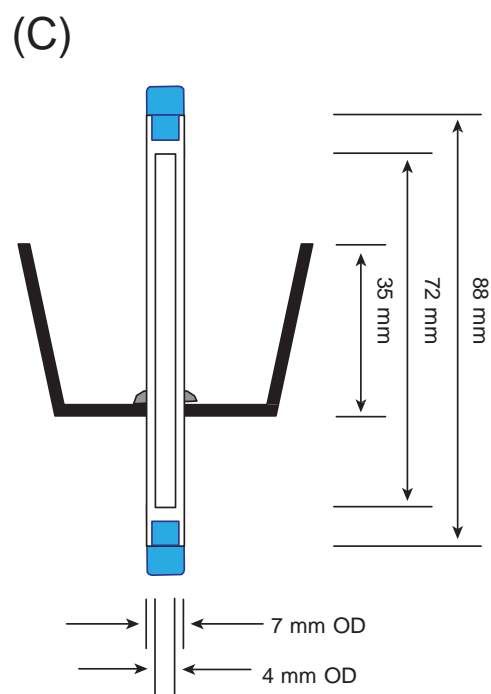
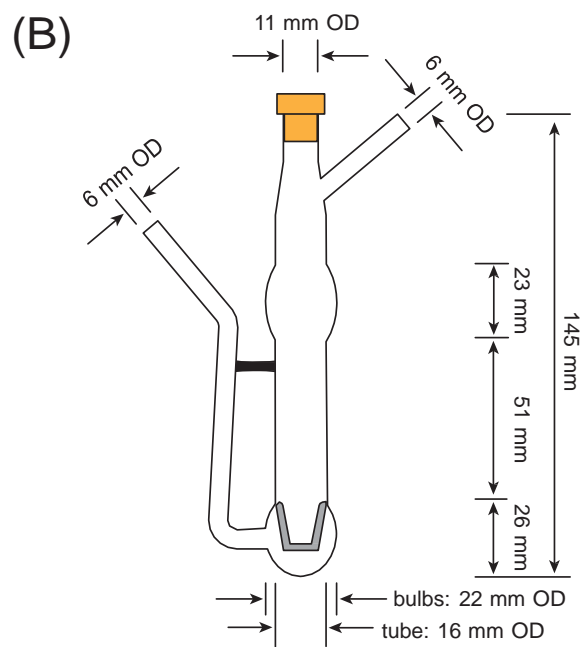
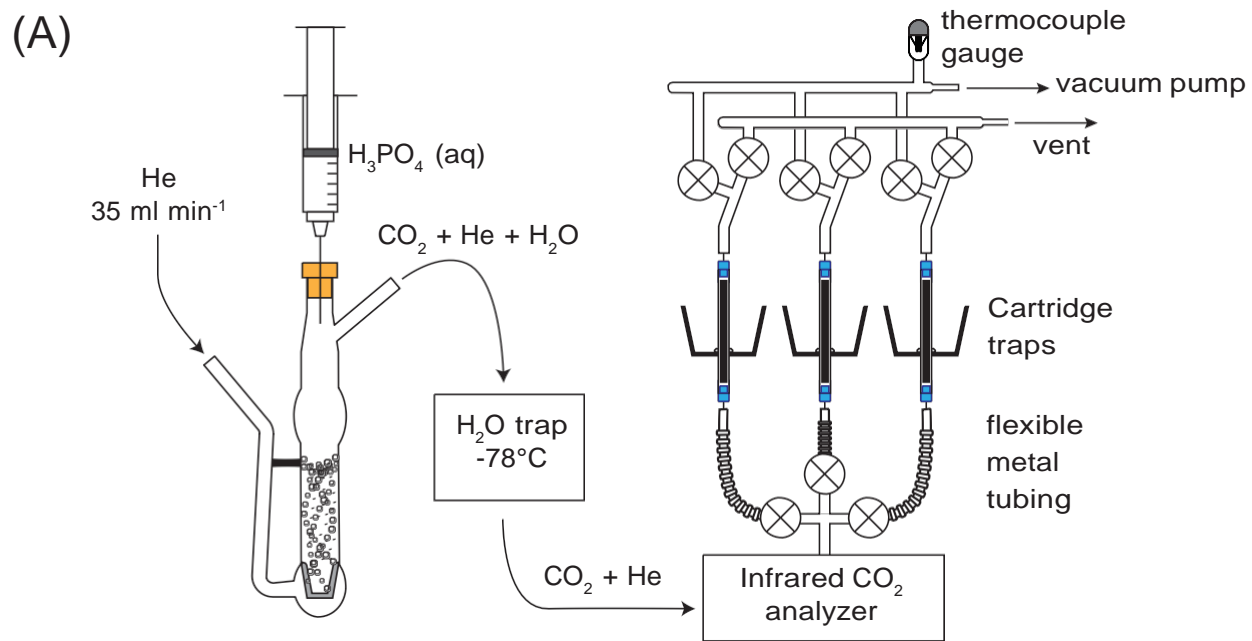


Figure 1

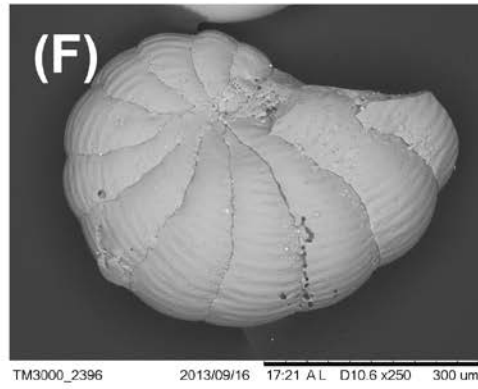
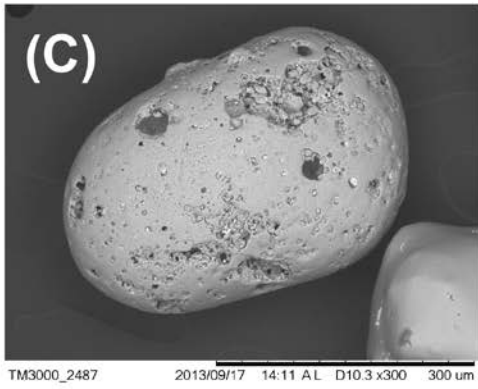
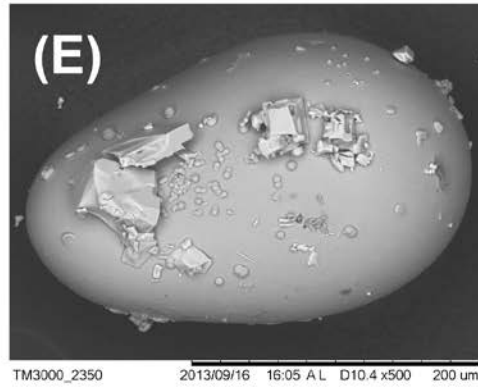
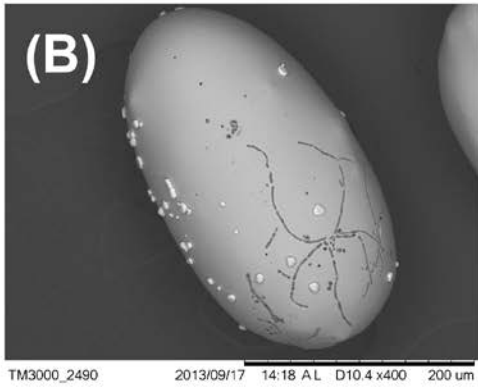
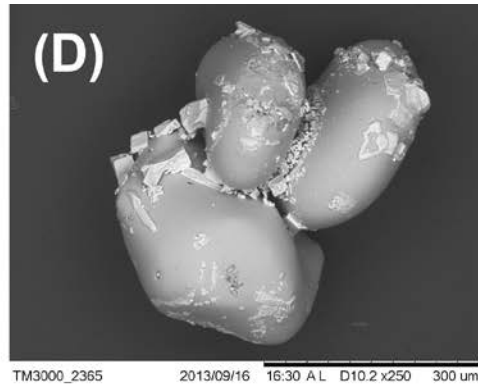
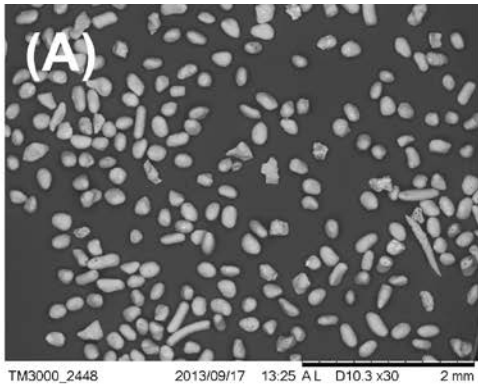


Figure 2

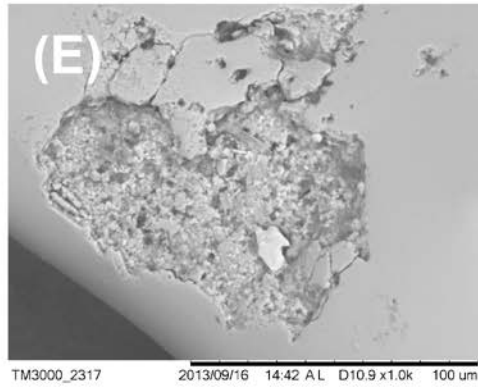
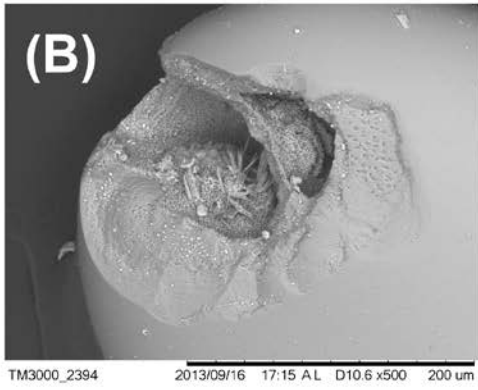
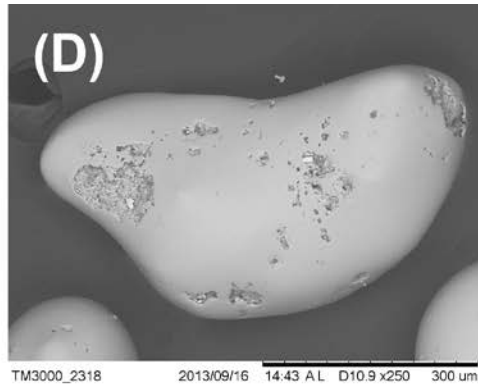
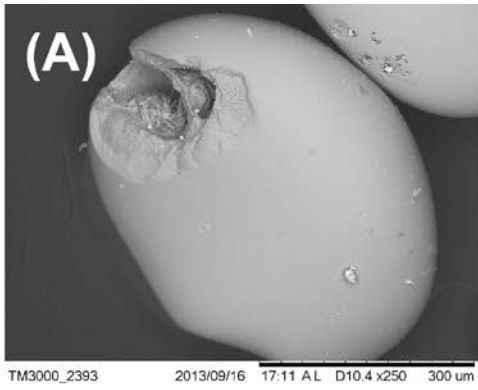


Figure 3

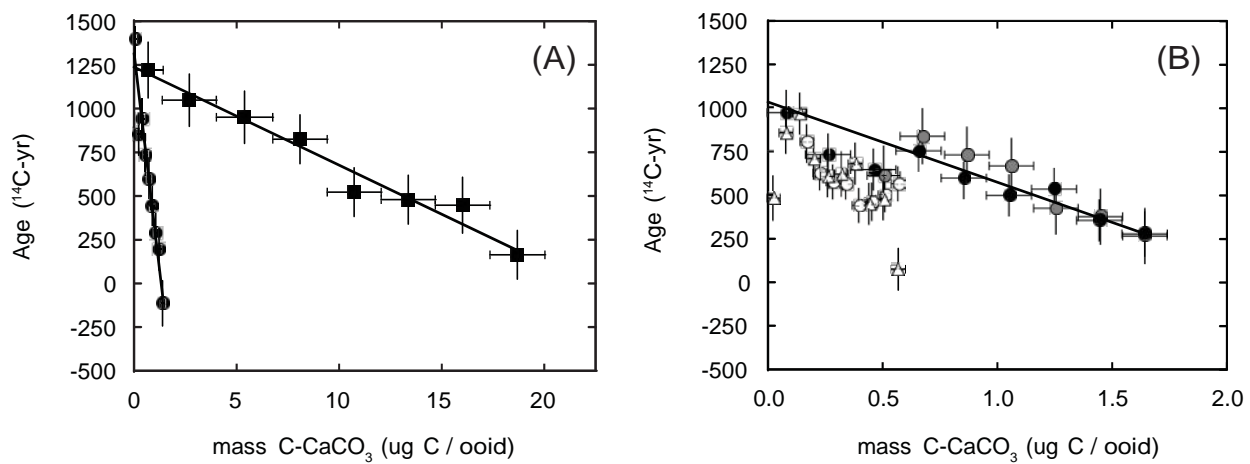


Figure 4

Appendix:

This appendix summarizes the data obtained in this experiment (Table A.1) and the approaches used to convert it into ^{14}C chronologies of individual, idealized ooids.

A. Radial ^{14}C ooid chronology approach

The following equations were used to generate radial ^{14}C chronologies of individual ooids from direct measurements of the masses and ^{14}C ages of large fractions of CO_2 released during acidification of multiple ooids. Uncertainties in all calculated values were propagated from their corresponding terms as single standard deviations. For brevity, the uncertainty equations have been omitted from this discussion.

A.1. Radial ^{14}C ooid chronologies as a function of carbonate mass.

The average initial mass of an individual ooid, \overline{M} , was estimated by multiplying its measured density, $\rho_{\text{ooid},R}$, by the volume of a sphere with an initial radius, R , inferred from sieving.

$$\overline{M} = \rho_{\text{ooid},R} \frac{4}{3} \pi R^3 \quad (\text{A.1})$$

Accordingly, the average number of ooids, n , in a sample was equal to the measured mass of all ooids in the sample, m_{sample} , divided by the average mass of an individual ooid, \overline{M} .

$$n = \frac{3m_{\text{sample}}}{\rho_{\text{ooid},R} 4\pi R^3} \quad (\text{A.2})$$

Therefore, the average mass of carbon, \overline{m}_i , acidified from layer i of an individual ooid was equal to the mass of carbon evolved from multiple ooids, as measured in the corresponding fraction of CO₂, $m_{f,i}$, divided by the average number of ooids in the sample, n .

$$\overline{m}_i = \frac{m_{f,i}}{n} \quad (\text{A.3})$$

Substituting Eq. A.2 into Eq. A.3 produced an equation for estimating this mass from the inferred value of R and direct measurements of $\rho_{\text{ooid},R}$, $m_{f,i}$, and m_{sample} .

$$\overline{m}_i = \rho_{\text{ooid},R} \frac{m_{f,i}}{m_{\text{sample}}} \frac{4}{3} \pi R^3 \quad (\text{A.4})$$

Assuming all carbonates from all ooids were liberated when the acidification ceased to produce CO₂, and that all CO₂ was captured without interruption, then each fraction of CO₂ originated from adjacent layers of carbonate. By this convention, the final fraction collected corresponded to the innermost layer of the cortex ($i = 1$). Accordingly, the boundary between this layer and the surface of the stony nucleus was defined as $\overline{m}_o = 0$. The total masses of carbonate carbon, $m_{r,j}$, contained within hypothetical spherical boundaries of radius, r , were calculated by sequentially adding the masses of each spherical layer in order from the innermost ($i = 1$) to the outermost ($i = N$) layers.

$$m_{r,j} = \sum_{i=1}^j m_i \quad (\text{A.5})$$

Since the measured conventional ¹⁴C ages were, by definition, mass-weighted average ages for all C atoms in each fraction, they were associated with a corresponding average mass for each layer, i.e., at the midpoint mass of each spherical layer, $\overline{m}_{r,j}$.

$$\overline{m_{r,j}} = \frac{\overline{m_j}}{2} + \sum_{i=1}^j \overline{m_{i-1}} \quad (\text{A.6})$$

The difference between the total mass of all ooids in a sample and the stoichiometrically equivalent mass of all CaCO_3 liberated as CO_2 by exhaustive acidification was attributed to the presence of stony nuclei, inorganic inclusions, and organic inclusions. If these inclusions were a small proportion of the non- CaCO_3 constituents, then the residual mass represented an upper limit on the total mass of all stony nuclei in the sample and may be expressed as a percentage (Table 1).

However, an unknown proportion of the ooids' mass may have consisted of CaCO_3 nuclei (e.g., fossil forams) that would have been acidified and collected with cortical CO_2 . Therefore, a lower limit on the average mass *per individual nucleus* may be obtained by dividing the residual mass by the number of ooids in the sample.

A.2. Ooid growth model: constant net growth rate with respect to mass

The simplest model of ooid growth assumes that the mass of carbonate-carbon, m_c , increased at a constant net rate, k_m , during sufficiently long periods of time, t . Each successive layer of assimilated carbonate would have recorded the ^{14}C abundance of its carbon source and then undergone radioactive decay. The innermost layer of carbonate should therefore possess the greatest ^{14}C age, T_{max} , when assuming constant reservoir ages and well-preserved cortices. Hence, the net growth rate (Eq. A.7) can be expressed in terms of ^{14}C ages, T , rather than the forward passage of time, by inclusion of a negative sign in the rate expression.

$$-\frac{dm_c}{dT} = k_m \quad (\text{A.7})$$

Integrating Eq. A.7 as a variable-separable differential equation from $m_c = 0$ and $T = T_{max}$ to $(m_c = m_r$ and $T = T_r$ predicts a continuous, linear relationship between ^{14}C ages, T_r , of an infinitesimally thin lamination that coats a spherical mass of carbon, m_r , with radius, r .

$$T_r = T_{max} - \frac{1}{k_m} m_r \quad (\text{A.8})$$

In practice, the ^{14}C ages are measured from discrete fractions of CO_2 etched from layers of carbonate with non-trivial thickness. Since they represent the average ^{14}C ages of all carbon in each layer, \overline{T}_j , they should be plotted against the mass-weighted average mass of carbon for each fraction, $\overline{m}_{r,j}$ (from Eq. A.6) according to Eq. A.9.

$$\overline{T}_j = T_{max} - \frac{1}{k_m} \overline{m}_{r,j} \quad (\text{A.9})$$

If the mass of oolitic carbonate grew at a constant net rate, then a plot of ^{14}C ages versus corresponding masses will yield a straight line, whose slope and intercept empirically reveal the ooids' mean net growth rate, k_m , and limiting maximum ^{14}C age, T_{max} , respectively.

A.3. *Maximum lifespan based on constant net growth rate in carbonate mass*

Assuming a constant local reservoir age, the minimum time between ooid genesis and either sample collection or cessation of ooid growth was calculated as the ^{14}C age difference between the innermost and outermost fractions (i.e., the “lifespan”). The maximum lifespan was estimated by subtracting the limiting ^{14}C age of the outermost, infinitesimally thin lamination (i.e., Eq. A.9 at $\overline{m}_{r,j} = \Sigma \overline{m}_i$ for all $i = 1$ to N layers) from the ^{14}C age of the innermost

infinitesimally thin lamination, T_{max} . The T_{max} terms cancel when calculating this difference, simplifying the expression for maximum lifespan to the total mass of carbonate-carbon in an ooid divided by its mean net growth rate.

$$\text{maximum lifespan} = \frac{1}{k_m} \sum_{i=1}^N \overline{m}_i \quad (\text{A.10})$$

If the value of k_m is determined by geometric mean model-II linear regression on a plot of conventional ^{14}C ages, then the maximum lifespan does not depend on inferred value of R or the measured values of ρ_{ooid} or m_{sample} . That is, uncertainty in the maximum lifespan is minimized to a function of the measured masses and ^{14}C ages in each fraction of CO_2 evolved from the reactor, as follows. First, the summation in Eq. A.10 can be expressed in terms of the mass of carbon measured in each fraction of CO_2 based on Eq. A.3.

$$\text{maximum lifespan} = \frac{1}{k_m} \frac{1}{n} \sum_{i=1}^N m_{f,i} \quad (\text{A.11})$$

The $1/k_m$ term should be determined as the geometric mean slope of Eq. A.9, because both the masses and ^{14}C ages are measurements with non-trivial uncertainties. The geometric mean slope of Eq. A.9 can be calculated directly from slopes of model-I regressions of plots of \overline{T}_j versus $\overline{m}_{r,j}$, and of $\overline{m}_{r,j}$ versus \overline{T}_j (Eq. A.12, after Glover et al., 2011).

$$-\frac{1}{k_m} = \sqrt{\frac{\text{slope}_{\overline{T}_j \text{ on } \overline{m}_{r,j}}}{\text{slope}_{\overline{m}_{r,j} \text{ on } \overline{T}_j}}} \quad (\text{A.12})$$

Expanding the slope terms with equations for model-I least-squares linear regressions and cancelling like terms reveals that the set of masses, $\overline{m}_{r,j}$, reside in the denominator of the geometric mean slope equation.

$$\frac{1}{k_m} = - \sqrt{\frac{N \sum_{j=1}^N \overline{T_j^2} - \frac{\#}{\%} \sum_{j=1}^N \overline{T_j} \&^2}{N \sum_{j=1}^N \overline{m_{r,j}^2} - \frac{\#}{\%} \sum_{j=1}^N \overline{m_{r,j}} \&^2}} \quad (\text{A.13})$$

Substituting Equations A.3 and A.6 for $\overline{m_{r,j}}$ in Eq. A.13 and simplifying shows that the slope is primarily based on the relationship between measurements of each fraction's mass and ^{14}C age, and secondarily scaled by the calculated number of ooids, n (Eq. A.2), in the sample.

$$\frac{1}{k_m} = -n \cdot \sqrt{\frac{N \sum_{j=1}^N \overline{T_j^2} - \frac{\#}{\%} \sum_{j=1}^N \overline{T_j} \&^2}{N \sum_{j=1}^N \overline{m_{f,j}^2} - \frac{\#}{\%} \sum_{j=1}^N \overline{m_{f,j}} \&^2}} \quad (\text{A.14})$$

However, substituting Eq. A.14 for $1/k_m$ in Eq. A.11 demonstrates that the maximum lifespan of an ooid under this model is only a function of the masses and ^{14}C ages measured in each fraction of CO_2 (Eq. A.15).

$$\text{maximum lifespan} = - \sum_{i=1}^N m_{f,i} \cdot \sqrt{\frac{N \sum_{j=1}^N \overline{T_j^2} - \frac{\#}{\%} \sum_{j=1}^N \overline{T_j} \&^2}{N \sum_{j=1}^N \overline{m_{f,j}^2} - \frac{\#}{\%} \sum_{j=1}^N \overline{m_{f,j}} \&^2}} \quad (\text{A.15})$$

Likewise, the geometric mean intercept, T_{max} , is independent of the values of ρ_{ooids} , m_{sample} , and R . It is calculated from Eq. A.9 using the geometric mean slope (i.e., $-1/k_m$) and the average

values of the sets of masses and ^{14}C ages.

$$T_{\max} = \frac{1}{N} \sum_{j=1}^N \overline{T_j} + \frac{1}{k_m} \frac{1}{N} \sum_{j=1}^N \overline{m_{r,j}} \quad (\text{A.16})$$

The $1/N$ -weighting factor enables cancelation of the n term that is introduced upon substituting Eq. A.14 for $1/k_m$. Thus, T_{max} is also a function of only the masses and ^{14}C ages measured in each fraction of CO_2 (Eq. A.17).

$$T_{\max} = \frac{1}{N} \sum_{j=1}^N T_j - \sum_{j=1}^N \frac{m_{f,j}}{2} + \sum_{i=1}^j m_{f,j-1} \left(\sqrt{\frac{N \sum_{j=1}^N T_j^2 - \left(\sum_{j=1}^N T_j \right)^2}{N \sum_{j=1}^N m_{f,j}^2 - \left(\sum_{j=1}^N m_{f,j} \right)^2} + \sum_{i=1}^j \frac{m_{f,i}}{2} + \sum_{i=1}^j m_{f,i-1}} \right) \quad (\text{A.17})$$

Table A.1: Fraction masses^a and ¹⁴C measurements (F_m and corresponding ¹⁴C ages) for each size class of acidified ooids. Total sample masses (mg ooids) and densities (g/ml) are listed parenthetically below each sample name.

ID #	Fraction #	Mass (μ g C)	F _m	¹⁴ C age (yr BP)
Carbla Beach, 0.177 – 0.250 mm diameter (40.83 \pm 0.02 mg ooids; 2.5 \pm 0.6 g/ml)				
OoidGB11-1	1	324 \pm 32	1.014 \pm 0.034	<i>modern</i>
OoidGB11-2	2	324 \pm 32	0.976 \pm 0.033	200 \pm 280
OoidGB11-3	3	330 \pm 33	0.965 \pm 0.032	290 \pm 270
OoidGB11-4	4	324 \pm 32	0.946 \pm 0.032	440 \pm 270
OoidGB11-5	5	324 \pm 32	0.928 \pm 0.031	600 \pm 280
OoidGB11-6	6	330 \pm 33	0.912 \pm 0.031	740 \pm 280
OoidGB11-7	7	324 \pm 32	0.890 \pm 0.030	940 \pm 270
OoidGB11-8	8	324 \pm 32	0.899 \pm 0.030	850 \pm 270
OoidGB11-9	9	276 \pm 28	0.840 \pm 0.029	1400 \pm 280
Carbla Beach, 0.250 – 0.590 mm diameter (33.76 \pm 0.02 mg ooids; 2.6 \pm 0.4 g/ml)				
OoidGB10-01	1	330 \pm 33	0.980 \pm 0.017	160 \pm 140
OoidGB10-02	2	328 \pm 33	0.946 \pm 0.018	450 \pm 160
OoidGB10-03	3	324 \pm 32	0.942 \pm 0.016	480 \pm 140
OoidGB10-04	4	324 \pm 32	0.937 \pm 0.016	520 \pm 140
OoidGB10-05	5	327 \pm 33	0.902 \pm 0.015	820 \pm 140
OoidGB10-06	6	339 \pm 34	0.888 \pm 0.016	950 \pm 150
OoidGB10-07	7	324 \pm 32	0.878 \pm 0.015	1050 \pm 150
OoidGB10-08	8	169 \pm 17	0.859 \pm 0.016	1220 \pm 160

Table A.1, continued...

Highborne Cay, 0.105 – 0.177 mm diameter
(42.26 ± 0.02 mg ooids; 2.5 ± 0.4 g/ml)

OoidGB12-1	1	324 ± 32	0.932 ± 0.011	560 ± 100
OoidGB12-2	2	324 ± 32	0.939 ± 0.012	500 ± 100
OoidGB12-3	3	324 ± 32	0.944 ± 0.012	460 ± 110
OoidGB12-4	4	324 ± 32	0.946 ± 0.011	440 ± 100
OoidGB12-5	5	324 ± 32	0.932 ± 0.010	560 ± 90
OoidGB12-6	6	324 ± 32	0.931 ± 0.011	580 ± 100
OoidGB12-7	7	324 ± 32	0.925 ± 0.011	630 ± 100
OoidGB12-8	8	324 ± 32	0.905 ± 0.011	800 ± 100

Highborne Cay, 0.105 – 0.177 mm diameter replicate
(39.94 ± 0.02 mg ooids; 2.5 ± 0.4 g/ml)

OoidGB13-01	1	328 ± 33	0.991 ± 0.015	80 ± 120
OoidGB13-02	2	345 ± 34	0.942 ± 0.014	480 ± 120
OoidGB13-03	3	324 ± 32	0.945 ± 0.013	450 ± 120
OoidGB13-04	4	324 ± 32	0.919 ± 0.014	680 ± 120
OoidGB13-05	5	324 ± 32	0.926 ± 0.014	620 ± 130
OoidGB13-06	6	324 ± 32	0.927 ± 0.014	610 ± 120
OoidGB13-07	7	328 ± 33	0.916 ± 0.013	710 ± 120
OoidGB13-08	8	324 ± 32	0.887 ± 0.013	960 ± 120
OoidGB13-09	9	324 ± 32	0.899 ± 0.013	850 ± 120
OoidGB13-10	10	282 ± 28	0.942 ± 0.014	480 ± 130

Table A.1, continued...

Highborne Cay, 0.177 – 0.250 mm diameter
(34.36 ± 0.02 mg ooids; 2.6 ± 0.6 g/ml)

OoidGB8-1	1	325 ± 33	0.966 ± 0.015	280 ± 130
OoidGB8-2	2	325 ± 33	0.957 ± 0.014	360 ± 120
OoidGB8-3	3	322 ± 32	0.936 ± 0.014	540 ± 120
OoidGB8-4	4	324 ± 32	0.940 ± 0.014	500 ± 120
OoidGB8-5	5	324 ± 32	0.928 ± 0.014	600 ± 120
OoidGB8-6	6	324 ± 32	0.911 ± 0.014	750 ± 120
OoidGB8-7	7	324 ± 32	0.923 ± 0.013	650 ± 120
OoidGB8-8	8	324 ± 32	0.913 ± 0.014	730 ± 120
OoidGB8-9	9	276 ± 28	0.886 ± 0.014	970 ± 130

Highborne Cay, ≤ 0.250 mm diameter
(34.90 ± 0.02 mg ooids; 2.5 ± 0.6 g/ml)

OoidGB6-1	1	324 ± 32	0.967 ± 0.019	270 ± 160
OoidGB6-2	2	324 ± 32	0.954 ± 0.019	380 ± 160
OoidGB6-3	3	324 ± 32	0.948 ± 0.018	430 ± 150
OoidGB6-4	4	324 ± 32	0.920 ± 0.017	670 ± 160
OoidGB6-5	5	324 ± 32	0.913 ± 0.017	730 ± 160
OoidGB6-6	6	324 ± 32	0.901 ± 0.017	840 ± 160
OoidGB6-7	7	240 ± 24	0.927 ± 0.019	610 ± 170

^a Masses were calculated from integrated, continuous photometric measurements of CO₂, for which we assumed an uncertainty of ≤ 10 %.